Analysis of Windshear from Airline Flight Data

R. E. Bach Jr.* and R. C. Wingrove*
NASA Ames Research Center, Moffett Field, California

Advanced analysis methods, applied to airline digital flight records and air traffic control radar tracking data, are providing new insight into atmospheric disturbances that cause serious operating problems for aircraft. Reviewed in this paper are performance-based methods for determining unmeasured flow angles and the possible influence of rain on lift and drag, and a state estimation procedure for determining winds along the flight path. The methods are applied to data records from the Delta Airlines flight 191 windshear accident at the Dallas-Ft. Worth Airport, Aug. 2, 1985, involving an L-1011 airliner on final approach. The results indicate that the aircraft encountered a strong downflow that exceeded 40 ft/s along with a headwind-to-tailwind change that exceeded 100 ft/s. The outflow near the ground was accompanied by large, rapid changes in vertical wind, consistent with the presence of imbedded vortices. Although rain was present in the "downburst," the analysis showed no evidence of rain causing a loss in aircraft performance.

Introduction

ATMOSPHERIC disturbances that affect airline operations can be studied by analyzing flight data recorded during typical encounters. In the past, such investigations were usually hampered by the lack of good data, but more recent turbulence incidents have involved modern airliners equipped with digital flight data recorders (DFDR). Data from a DFDR, together with ground-based air traffic control (ATC) radar records, comprise a measurement set approaching that available from flight test. Hence, it is feasible to determine aircraft performance in turbulence and to characterize the turbulence environment.

In assisting the National Transportation Safety Board (NTSB) in its investigations of turbulence encountered by DFDR-equipped airliners, NASA Ames researchers have applied a state estimation method to determine winds along the flight path.[1] Several of these encounters involved severe clear-air turbulence at cruise altitudes. Analyses of the data from these incidents indicate that the aircraft encountered vortex arrays, caused by the breakdown of windshear layers over thunderstorms or mountain ranges.[2-4] This type of turbulence phenomenon is illustrated in Fig. 1a.

A more hazardous type of atmospheric disturbance is a "downburst," which is a strong, concentrated downdraft that induces a high-velocity outflow, with imbedded vortices, near the ground.[5-7] A typical downburst is shown in Fig. 1b. Such a downburst encounter resulted in the loss of Delta Airlines flight 191 at Dallas-Ft. Worth Airport (DFW) on Aug. 2, 1985. In that accident, an L-1011 on final approach flew into a downburst and contacted the ground about one mile short of the runway. The authors, as members of the NTSB Performance Group investigating the accident, analyzed the available flight records in an effort to characterize the downburst environment. The results, published in the NTSB accident report,[8] are included in this paper. We note that other analyses of this downburst have also been published.[9-12]

Current research on operational hazards suggests that heavy rain may adversely affect aircraft performance,[13-15] so a companion study was undertaken to detect possible effects of rain in the DFW downburst. L-1011 performance data were used, along with the DFDR flight records from the accident, to predict lift and drag time histories, which were then compared with the corresponding lift and drag derived from DFDR force measurements. Any significant differences might be attributable to rain effects. The results of this study are also included in this paper.

This paper describes the analysis of airline flight data to determine performance and winds and illustrates the methodology with the flight 191 downburst encounter. The next section describes the process of merging and synchronizing the flight data; subsequent sections outline the performance calculations and wind estimation procedures used in analyzing turbulence encounters. The results of the downburst investigations of flight 191 are presented in the final section. The state estimation method is described in the Appendix.

Flight Data Processing

The procedure used to determine winds along the flight path is the same, whether the turbulence encountered is associated with vortices at cruise altitude or with a downburst near the ground. In this procedure, which is outlined in Fig. 2, data from the DFDR and ATC radar records are synchronized and merged and the air data are corrected. Performance calculations are made to synthesize unmeasured time histories of angles of attack and sideslip. When a complete data set is in place, a state estimation algorithm is employed to estimate the winds. This section describes the processing required to

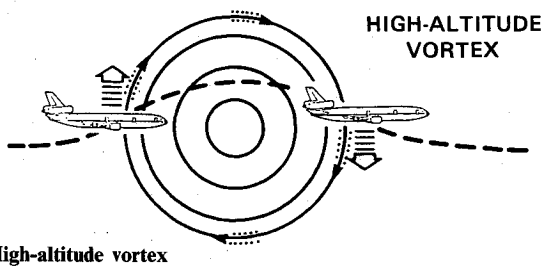

a) High-altitude vortex

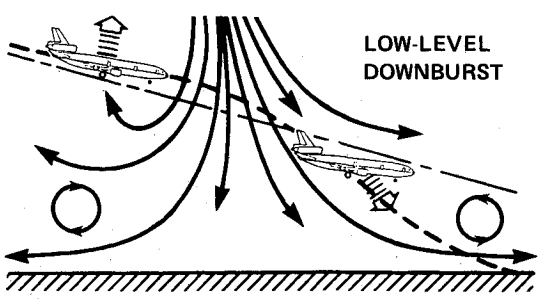

b) Low-level downburst

Fig. 1 Typical windshear disturbances.

Presented as Paper 86-2227CP at the AIAA Atmospheric Flight Mechanics Conference, Williamsburg, VA, Aug. 18–20, 1986; received Dec. 5, 1986; revision received Aug. 4, 1988.

*Aerospace Engineer. Member AIAA.

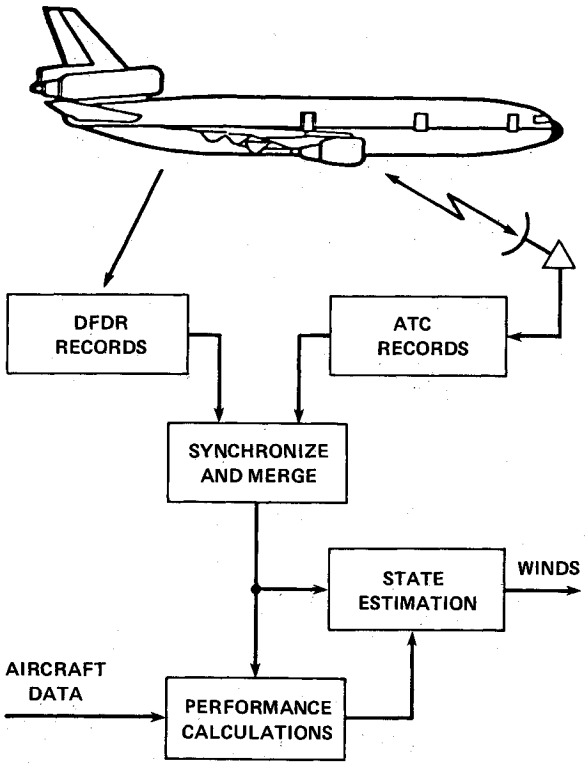

Fig. 2 Procedure for estimation of flightpath winds from airline flight records.

Table 1 Parameters in the L-1011 DFDR system

Record	Rate, Hz	Skew	Subframe no.
Vertical acceleration	4	12	1–4
Lateral acceleration	4	14	1–4
Longitudinal acceleration	4	1	1–4
Roll angle	1	16	1–4
Pitch angle	1	50	1–4
Heading angle	1	2	1–4
Indicated airspeed	1	18	1–4
Angle of attack (left vane)	2	10	1–4
Angle of attack (right vane)	2	24	1–4
Pressure altitude	1	4	1–4
Air temperature	0.5	54	2,4
Stabilator deflection	1	39	1–4
Rudder deflection	2	26	1–4
Thrust (engine 1)	0.25	32	1
Thrust (engine 2)	0.25	32	2
Thrust (engine 3)	0.25	32	3

prepare the data set for performance calculations and wind estimation.

Data from a DFDR include measurements (typically sampled at intervals of 0.25–4.0 s) of accelerations, Euler angles, pressure altitude, airspeed, and other variables. The important recorder parameters for an L-1011 DFDR system are shown in Table 1. The "frame" duration for the system is 4 s; there are four "subframes" in each frame and each subframe has 64 sampling "slots." The column headed "rate" defines the basic sampling rate for each parameter; the one headed "skew" defines the delay (in 1/64 s intervals) from the start of a subframe until the parameter is first sampled. The last column specifies the subframe(s) in which the sample appears. For example, a parameter sampled at a rate of 4 Hz, with a skew of 14, would occupy slots 14, 30, 46, and 62 in each subframe. However, a parameter sampled at a rate of 0.25 Hz with a skew of 32 would occupy slot 32 in only one subframe of each frame.

The first step in processing the DFDR data is to interpolate each measured parameter at the highest sampling rate (usually 4 Hz) before performing air data corrections and other calculations. The interpolation is accomplished with a digital filtering algorithm operating at a rate of 64 Hz in order to properly accommodate parameter skews. The filter also provides Euler angle time-derivative estimates for use in computing the body angular rates needed for estimating angles of attack and sideslip (or for correcting vane angles). After filtering, each parameter is down-sampled from 64 Hz to the appropriate rate (4 Hz) and the aforementioned calculations are performed.

The second step is to correctly merge the DFDR data with the ATC radar data. Although each data source is time tagged, there may be an absolute timing error of several seconds on either (or both) of the sources. However, usually included with the radar track is an independent (transponded) record of the aircraft's pressure altitude, which can be compared with the DFDR altitude record for time synchronization of the sources. Since the encoding altimeter for the transponder registers on increments of 100 ft, a fairly large change in altitude is necessary for synchronizing the sparsely sampled radar track with the 1 Hz DFDR altimeter measurement record.

The last step in data processing prior to performance calculations or wind estimation is to make the usual air data computations.[16] These include calculations of Mach number, dynamic pressure, true airspeed, and correction of the flow angle for upwash and pitch rate to obtain the angle of attack (when the flow angle is included with the DFDR records). It should be noted that the angle-of-attack time history is essential in determining vertical wind in an investigation of a severe turbulence encounter.

Performance Calculations

The time histories of force coefficients derived from flight data can be quite useful in accident investigations. The lift coefficient can be employed to estimate angle of attack α when that record is not among DFDR measurements[17]; a similar procedure is generally used to reconstruct the sideslip angle β from a time history of the side force coefficient. Both lift and drag are used in studies of possible performance degradation that might be caused by heavy rain or ice. This section reviews the use of performance calculations in analyzing turbulence encounters.

Aircraft force coefficients can be expressed in two ways. In the first, the actual lift, drag, and side force coefficients are given in terms of measurements of body axis accelerations (a_x,a_y,a_z) and thrust components (T_x,T_y,T_z) by

$$C_L = [(ma_x - T_x)\sin\alpha - (ma_z - T_z)\cos\alpha]/QS \quad (1)$$

$$C_D = -[F\cos\beta + (ma_y - T_y)\sin\beta]/QS \quad (2)$$

$$C_C = [F\sin\beta - (ma_y - T_y)\cos\beta]/QS$$

$$F = (ma_x - T_x)\cos\alpha - (ma_z - T_z)\sin\alpha \quad (3)$$

where m is the aircraft mass, Q the dynamic pressure, and S the wing area. The thrust is determined from tabular data relating the actual thrust to the particular engine parameter recorded.

A second set of expressions for the force coefficients is obtained by specifying corresponding aerodynamic models of the form

$$C_L = C_L(\alpha,M) + \sum_i l_i \quad (4)$$

$$C_D = C_D(\alpha,M) + \sum_i d_i \quad (5)$$

$$C_C = C_C(\beta,M) + \sum_i y_i \quad (6)$$

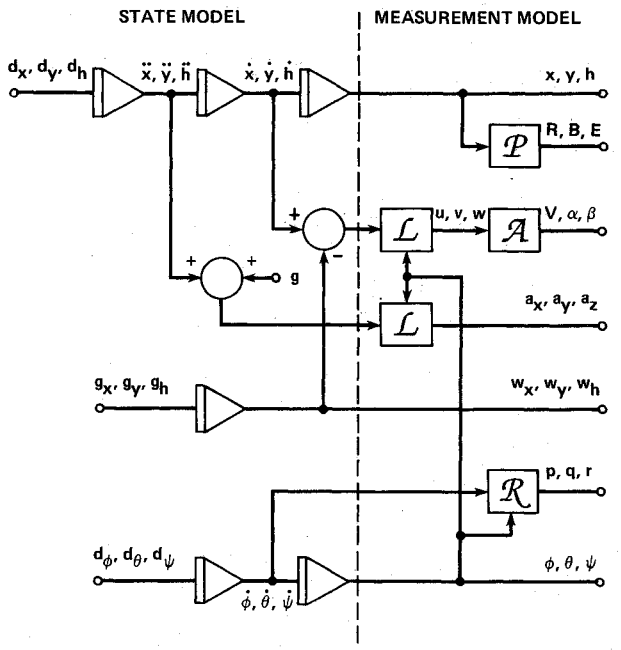

Fig. 3 State and measurement models for the SMACK state estimation procedure.

where M is the Mach number. Terms forming the sums in Eqs. (4–6) represent the contributions of angular rates, flaps, spoilers, control surfaces, landing gear, and ground effect. It should be emphasized that, in general, the coefficient models represent all that is known about the aerodynamic properties of the aircraft from theoretical predictions, wind-tunnel experiments, and flight testing.

For the application of estimating an angle-of-attack time history, the lift coefficient expressions of Eqs. (1) and (4) are equated, giving a nonlinear algebraic equation to be solved for angle of attack at each time point. An iterative procedure like the Newton-Raphson method works very well for this problem.[17] A similar technique is used with side force coefficient expressions for estimating the sideslip angle. In the analysis of the flight 191 data described later in this paper, measured flow angles (left and right alpha vanes) were used to derive angle of attack, whereas the coefficient method was used to estimate the angle of sideslip (beta-vane measurements are not included with DFDR records).

In another application, the investigation of possible performance degradation caused by heavy rain, time histories of lift and drag generated from Eqs. (1) and (2) are compared to the corresponding time histories predicted by the coefficient models of Eqs. (4) and (5). In the regions where the measured lift (or drag) values are consistently lower (or higher) than predicted and where rain was known to exist, a degradation in aircraft performance may be inferred.

Flight Path Winds

A technique known as state estimation can be used with data from several sources (e.g., flight recorder, ATC radar) to determine the winds along an aircraft's flight path. The method is general and independent of specific aircraft performance parameters; the basic procedure is outlined in the Appendix. Wind estimation in turbulence encounters is performed using an aircraft state estimation program called SMACK (Smoothing for Aircraft Kinematics), developed at NASA Ames Research Center.[18] In this program, aircraft motions are governed by a six-degree-of-freedom kinematic model, referenced to a flat, nonrotating Earth. Choice of a set of state variables consisting of Euler angles (ϕ,θ,ψ), inertial positions (x,y,h), and their time derivatives leads to the linear state model shown in Fig. 3. For wind estimation, the state model must be augmented with wind states (w_x,w_y,w_h). Note

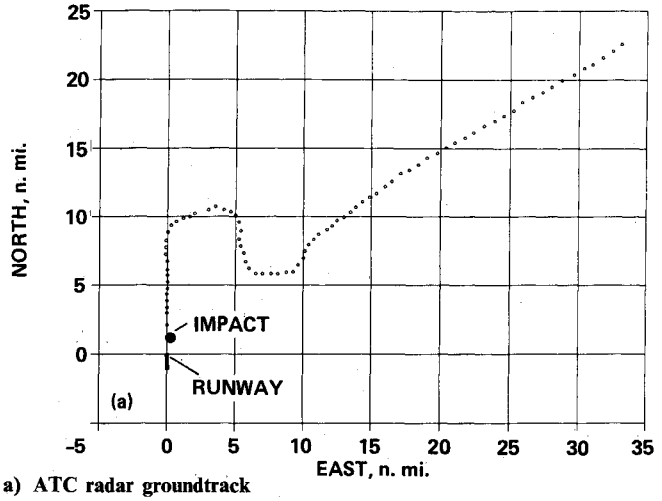

a) ATC radar groundtrack

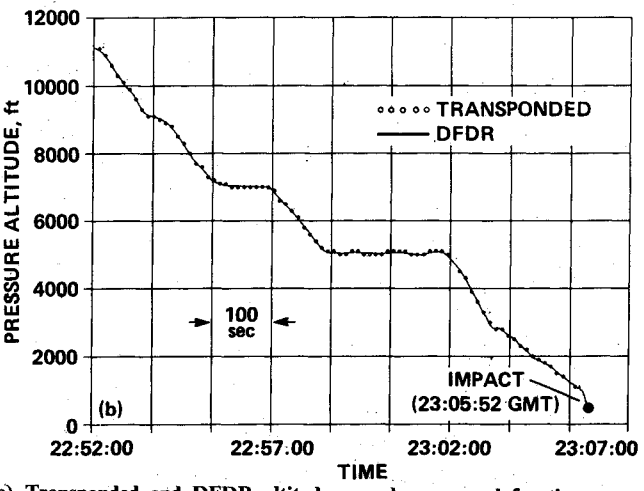

b) Transponded and DFDR altitude records compared for time synchronization

Fig. 4 Flight 191 approach to DFW.

that the block symbols to the left of the vertical dashed line represent integrators.

All nonlinearities associated with aircraft kinematics appear in the measurement model. For example, the aircraft angular velocities (p,q,r) are expressed in terms of the states as

$$p = \dot{\phi} - \dot{\psi}\sin\theta \tag{7}$$

$$q = \dot{\psi}\sin\phi\cos\theta + \dot{\theta}\cos\phi \tag{8}$$

$$r = \dot{\psi}\cos\phi\cos\theta - \dot{\theta}\sin\phi \tag{9}$$

Equations (7–9) are computed in the block of Fig. 3 labeled R. Calculations of aircraft body axis velocities (u,v,w) and specific forces (a_x,a_y,a_z) require the usual transformations from earth to body coordinates,[18] which are performed in the blocks labeled $\mathfrak{L}$. Radar variables R (slant range) and B (bearing angle), where

$$R = (x^2 + y^2 + h^2)^{1/2}, \qquad B = \tan^{-1}(y/x) \tag{10}$$

and aerodynamic variables V (airspeed), α (angle of attack), and β (sideslip angle), where

$$V = (u^2 + v^2 + w^2)^{1/2} \tag{11}$$

$$\alpha = \tan^{-1}(w/u), \qquad \beta = \sin^{-1}(v/V) \tag{12}$$

are calculated in the blocks labeled $\mathscr{P}$ and $\mathscr{A}$, respectively.

To solve the aircraft flight path wind problem discussed in the next section, two procedures were considered. The first would use SMACK to determine the integrator initial condi-

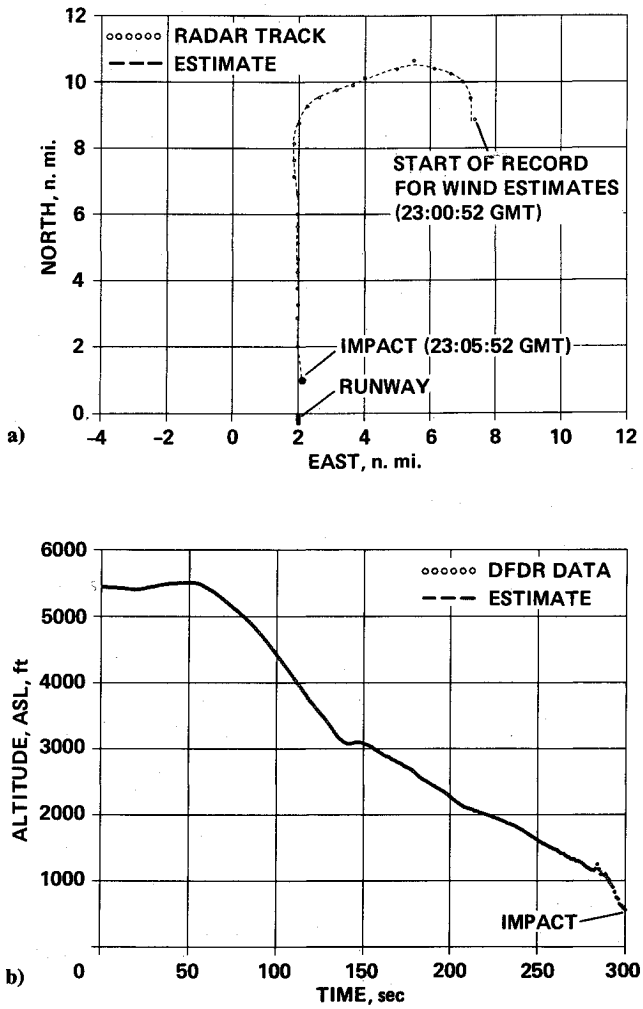

Fig. 5 Position solutions for 5 min: a) ground track; b) pressure altitude.

tions, accelerometer biases, and forcing-function time histories (d_x,d_y,d_h), (d_ϕ,d_θ,d_ψ), and (g_x,g_y,g_h) that provide the "best fits" to the measurement records (x,y,h), (ϕ,θ,ψ), (V,α,β), and (a_x,a_y,a_z). The wind estimates (w_x,w_y,w_h) along the flight path are obtained as part of the SMACK solution. A second procedure would fit only the inertial data using SMACK and then calculate the wind components separately from

$$w_x = \dot{x} - V\cos\theta_w\cos\psi_w \tag{13}$$

$$w_y = \dot{y} - V\cos\theta_w\sin\psi_w \tag{14}$$

$$w_h = \dot{h} - V\sin\theta_w \tag{15}$$

where the wind axis Euler angles (θ_w,ψ_w) are given by

$$\theta_w = \sin^{-1}(\cos\alpha\cos\beta\sin\theta - C\cos\theta) \tag{16}$$

$$\psi_w = \psi + \tan^{-1}[(\sin\beta\cos\phi - \sin\alpha\cos\beta\sin\phi)/D] \tag{17}$$

where

$$C = \sin\alpha\cos\beta\cos\phi + \sin\beta\sin\phi$$

$$D = \cos\alpha\cos\beta\cos\theta + C\sin\theta$$

Because the air data variables (V,α,β) derived from the flight 191 DFDR were relatively "smooth," the second procedure was used to obtain the wind estimates presented in the next section.

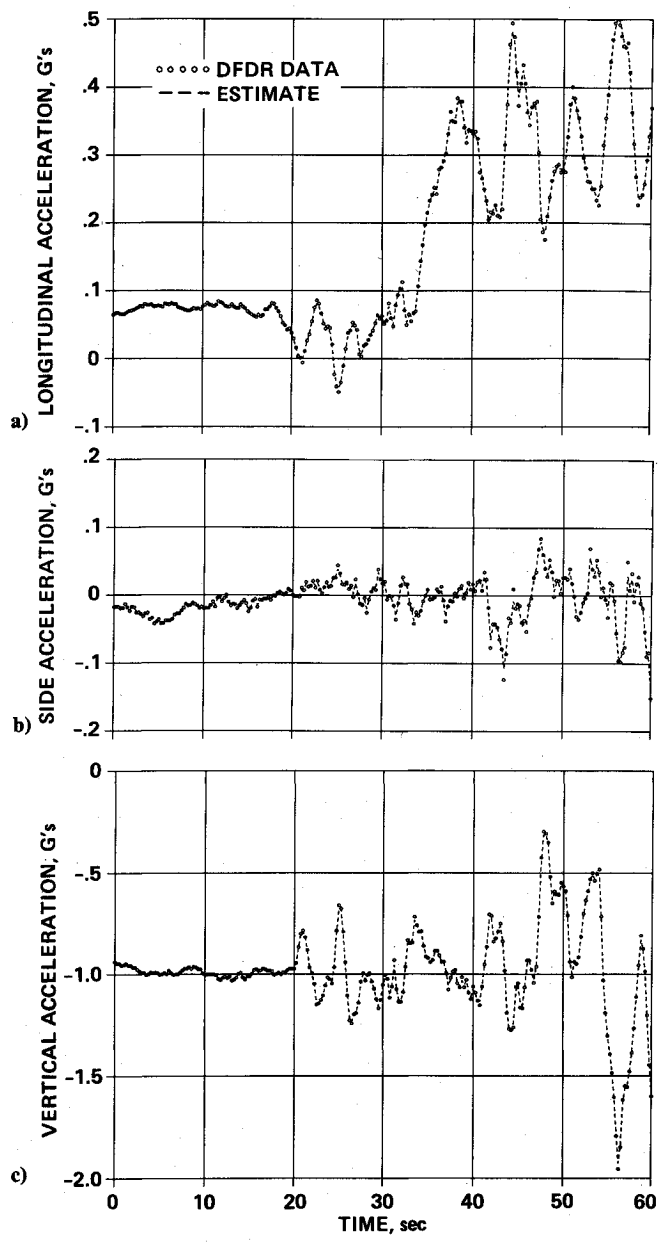

Fig. 6 Acceleration solutions (final 60 s): a) X-body axis, b) Y-body axis, c) X-body axis.

Flight 191 Accident

The Delta Airlines flight 191 accident occurred during an attempted landing at the Dallas-Ft. Worth Airport. A plan view of the approach path of the L-1011 aircraft as measured by ATC radar is shown in Fig. 4a. These 14 min of radar data show the aircraft approaching from the northeast and turning south onto the final glidepath to the runway. The point of initial contact with the ground (solid circle) is at a location 360 ft to the east and 6343 ft to the north of the runway origin. Shown in Fig. 4b for the same time interval are two curves of pressure altitude that represent the "best fit" of the DFDR record to the transponded record. The time shift required to synchronize the two data sources was 1 s.

After the data were synchronized and the true airspeed, angle of attack (from the vanes), and sideslip angle (from the performance equations) were calculated, the state estimation program SMACK was applied to determine the winds. The kinematic equations were integrated over a 5 min period that started before the turn onto the final approach and ended with the initial ground contact. The fits to the position data for this period are shown in Fig. 5. In these figures, the small circles represent the measured values and the dashed lines

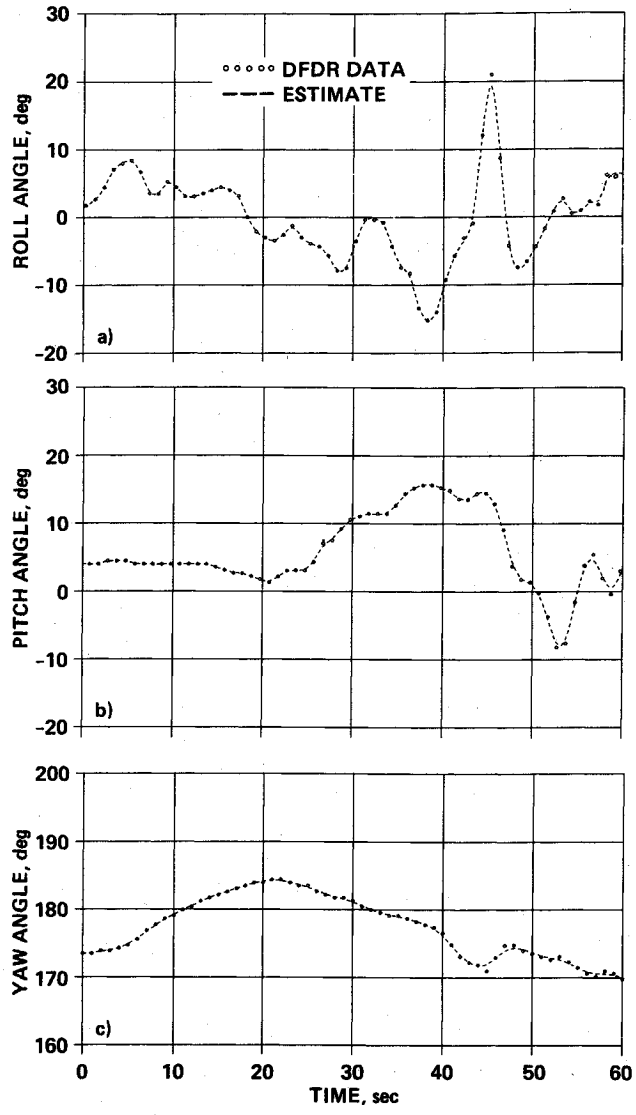

Fig. 7 Euler-angle solutions (final 60 s): a) roll, b) pitch, c) yaw.

represent the time histories generated by SMACK. Considering that the least count of the ATC tracking data is on the order of 1/8 n.mi., there is good agreement between the estimated path and the radar groundtrack (Fig. 5a). The inertial altitude estimate is shown with the DFDR barometric altitude record in Fig. 5b. During most of this 5 min interval, there is good agreement between the estimated inertial altitude and the measured barometric altitude. However, during the final portion (in the downburst), there is some discrepancy, apparently due to local pressure variations caused by the atmospheric disturbance.

Because the aircraft was in the downburst for less than a minute before its initial contact with the ground, the rest of the analysis described in this section will cover only the final 60 s of flight. Figure 6 shows the time histories of the three body axis accelerations and Fig. 7 the time histories of the three body axis Euler angles. Note that the plots of Figs. 6 and 7 include the SMACK-derived "best fits" to the DFDR data records. Figure 8 shows time histories of the aerodynamic variables (true airspeed, angles of attack, and sideslip). The angle of attack was computed from the average value of right and left vanes after correction for upwash and pitch rate. Since vane rate limiting (at about 19 deg/s) occurred during the last 20 s, the rapid excursions in angle of attack shown in Fig. 8b are probably attenuated. As outlined in a previous section, the angle of sideslip was computed from the measured side force [Eq. (3)] and predicted aerodynamics [Eq. (6)], which included terms for rudder deflection and yaw rate.

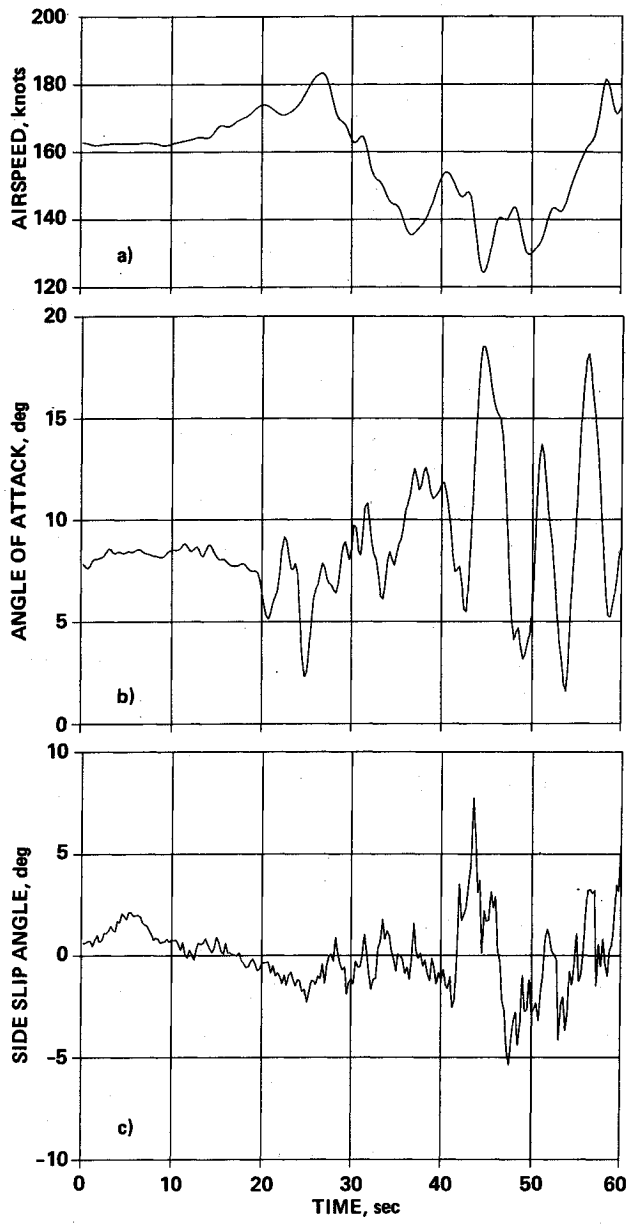

Fig. 8 Air data records (final 60 s): a) true airspeed, b) angle of attack, c) sideslip angle.

Figure 9a presents a time history of the aircraft heading angle shown with the groundtrack angle. The value observed for the groundtrack angle at the final time is 174 deg from true north. This estimate of track angle at the final time is in agreement with the orientation of landing gear marks found in the field where the aircraft first contacted the ground. Figure 9b presents a time history of true airspeed together with the estimated ground speed. The ground speed is seen to be increasing beyond 210 knots at the point of initial contact. Inspection of Fig. 9 indicates that during the final few seconds there appears to be a tailwind of about 60 ft/s (35 knots).

The general pattern of the winds can be deduced from Fig. 10, which shows the three components of the wind vector. The horizontal components are shown in Fig. 10a and the vertical component in Fig. 10b. The results indicate that the aircraft encountered a strong downflow for a time period of 20 s, followed by a rapid change in vertical wind direction, and then followed by further changes about 5 s apart. During the period of major downflow, the aircraft experienced vertical winds on the order of -10 to -40 ft/s. When the aircraft entered the downflow, the headwind increased from about 20 ft/s to more than 50 ft/s. Then, during a period of 26 s, there was a change to a tailwind of more than 50 ft/s.

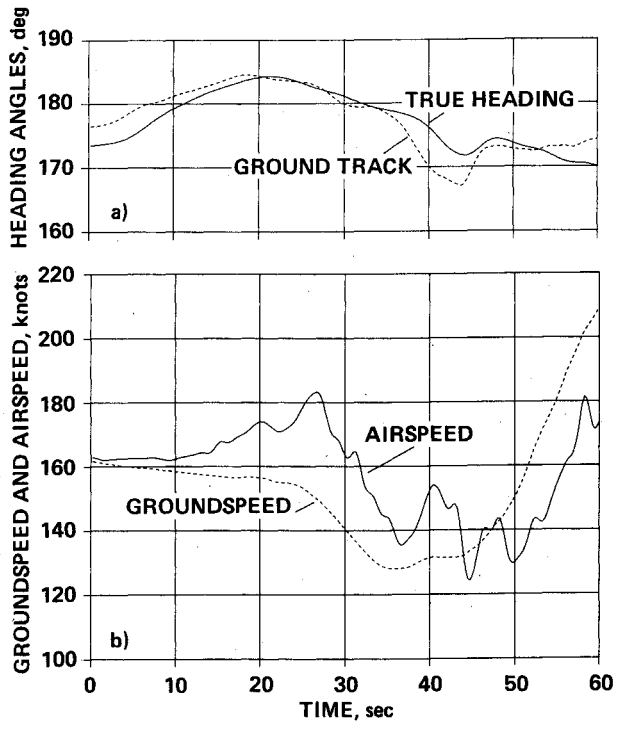

Fig. 9 Velocity estimates (final 60 s): a) true heading and ground track angles, b) true airspeed and ground speed.

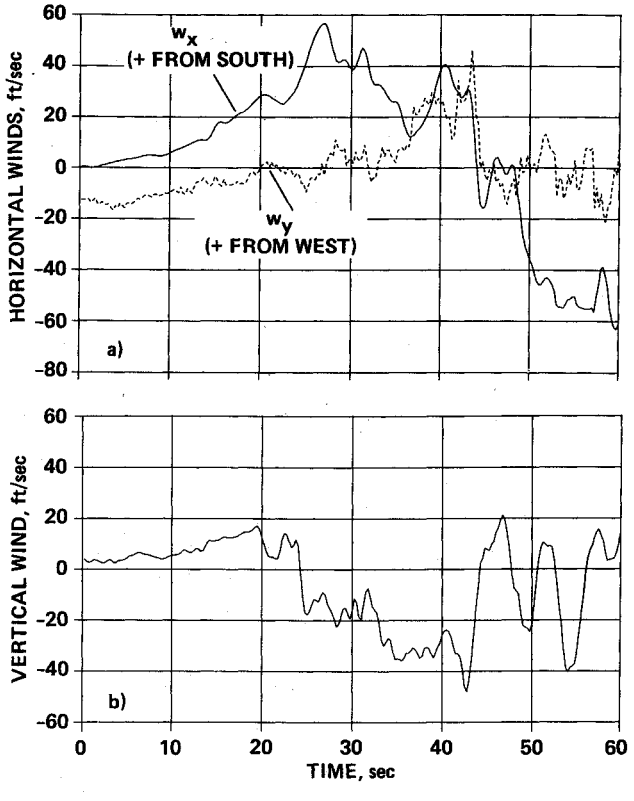

Fig. 10 Flightpath wind estimates (final 60 s): a) southerly and westerly components, b) vertical component.

Figure 11 shows winds along the flight path from different perspectives that clearly indicate the pattern of winds in the downburst. The diagram in Fig. 11a shows the flight path viewed from above with the wind arrows computed from the horizontal components w_x and w_y. These results show the changes in the magnitude and direction of the horizontal wind as the aircraft proceeds through the downburst. As shown by the rotation of the horizontal wind vector, the source of the

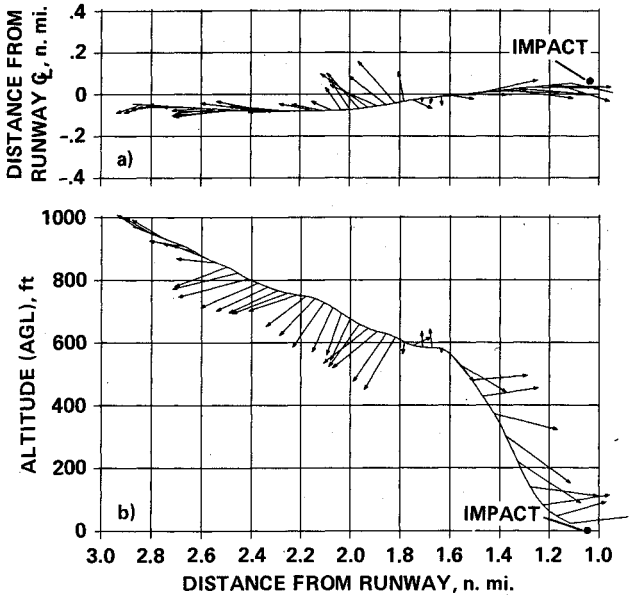

Fig. 11 Flight path wind vectors (final 44 s): a) seen from above, b) seen from the west.

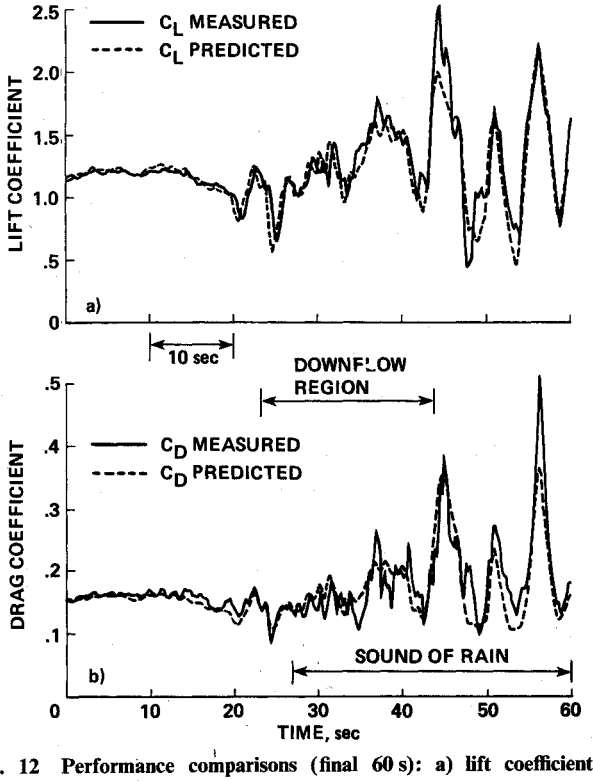

Fig. 12 Performance comparisons (final 60 s): a) lift coefficients, b) drag coefficients.

downflow appears to be west of the flight path. The diagram in Fig. 11b shows the flight path viewed from the west with the wind arrows computed from the w_x and w_h components. Following the downflow portion, both the outflow near the ground along with changes in the vertical wind are evident. The winds before and after the downflow indicate the presence of vortex rings.[12] According to the vortex ring model, when a ring impacts the surface, its circulation is spun up, providing a mechanism for the changes in vertical wind that are observed near the ground. In particular, the rapid changes just after the downflow are typical of a series of strong vortices.

Finally, for the investigation of possible performance degradation in the DFW accident, the time histories of lift and drag

coefficients are shown in Fig. 12, with the onset of rain noted. The cockpit voice recorder indicated that the sound of rain began shortly after the aircraft entered the downflow and continued until impact. Both the measured and the predicted coefficient values are shown so that a performance comparison can be made. The results show no significant differences between the measured and predicted time histories either before or during the period of rain, which suggests that rain was not a factor in degrading the performance of the L-1011.

Concluding Remarks

This paper has described methods being used to analyze airline encounters with severe turbulence from flight recorder and ATC tracking data. These included performance-based techniques for estimating both unmeasured flow angles and the possible influence of rain on lift and drag, and a state estimation technique for estimating winds along the flightpath. The methods were applied to the records from the Delta Airlines flight 191 accident at Dallas-Ft. Worth Airport. The analysis of this accident, which is one of the first involving an aircraft with an onboard digital recording system, provides a detailed look into the pattern of low-level windshear in a downburst environment.

The results indicate that at about 800 ft above the surface, the aircraft encountered a strong downflow for a period of 20 s, followed by a rapid change in vertical wind direction, and then followed by further changes about 5 s apart. During the period of major downflow, the aircraft experienced vertical winds in the range of -10 to -40 ft/s. When the aircraft entered the downflow, the headwind increased from about 20 to more than 50 ft/s. Then, during a period of 26 s, the headwind changed to a tailwind of more than 50 ft/s.

The wind patterns derived from the flight 191 records provide important new information to augment ongoing experiments and theoretical research on the downburst phenomenon. Furthermore, the estimated wind time histories provide a new set of data representing a severe downburst that can be used in simulation and pilot training.

Appendix: State Estimation

State estimation is a procedure that solves a state model

$$\dot{x} = f(x,w), \qquad x(t_0) = x_0 \tag{A1}$$

such that $h(x)$ in the measurement model

$$z = h(x) + v \tag{A2}$$

suitably matches the data record over an interval (t_0,t_f), usually in a least-squared error or minimum variance sense. In Eq. (A1), x is a vector of state variables and w a vector of forcing functions. In Eq. (A2), $h(x)$ is the vector of output variables; z and v are vectors representing the measurements and corresponding (random) measurement errors. Any bias or scale factor errors associated with either model are appended to the state vector and treated as constant but unknown parameters.

Solution of the state-estimation problem consists of determining x_0 and $w(t)$ to minimize the squared error performance measure:

$$J = (x_0 - \bar{x}_0)^t P_0^{-1}(x_0 - \bar{x}_0)/2 + \int_{t_0}^{t_f} \{w^t Q^{-1} w + [z - h(x)]^t R^{-1}[z - h(x)]\}\, dt/2 \tag{A3}$$

subject to the dynamic constraint of Eq. (A1). In Eq. (A3), $\bar{x}_0$ is an a priori estimate of x_0 and P_0, Q, and R are weighting matrices. Note that the first term of Eq. (A3) serves as a "penalty" function that tends to bias the estimate of x_0 toward its a priori value. An algorithm for the minimization of the performance measure is included in Ref. 18.

References

[1]Bach, R. E., Jr. and Wingrove, R. C., "Applications of State Estimation in Aircraft Flight Data Analysis," *Journal of Aircraft*, Vol. 22, July 1985, pp. 547–554.

[2]Parks, E. K., Bach, R. E., Jr. and Wingrove, R. C., "Analysis of the Nature and Cause of Turbulence Upset Using Airline Flight Records," Thirteenth Annual Symposium of the Society of Flight Test Engineers, New York, Sept. 1982.

[3]Parks, E. K., Wingrove, R. C., Bach, R. E., Jr. and Mehta, R. S., "Identification of Vortex-Induced Clear-Air Turbulence Using Airline Flight Records," *Journal of Aircraft*, Vol. 22, Feb. 1985, pp. 124–129.

[4]Mehta, R. S., "Modeling Clear-Air Turbulence with Vortices Using Parameter-Identification Techniques," *Journal of Guidance, Control, and Dynamics*, Vol. 10, Jan.-Feb. 1987, pp. 27–31.

[5]Caracena, F., "Is the Microburst a Large Vortex Ring Imbedded in a Thunderstorm Downdraft?," *Eos Transactions*, American Geophysical Union, Vol. 63, No. 45, 1982, p. 899.

[6]National Academy of Sciences, *Low-Altitude Windshear and its Hazard to Aviation*, National Academy Press, Washington, DC, 1983.

[7]Fujita, T. T., "The Downburst," Satellite and Mesometeorology Research Project Research Paper 210, University of Chicago, Chicago, 1985 (NTIS PB 85-148880).

[8]"Delta Airlines, Inc., Lockheed L-1011-3851-1, N726DA, Dallas/Ft. Worth International Airport, Texas, August 2, 1985," National Transportation Safety Board, Washington, DC, Rept. NTSB/AAR-86/05, 1986.

[9]Bray, R. S., "Aircraft Performance in Downburst Windshear," *Windshear*, Society of Automotive Engineers, Warrendale, PA, SP-681, 1986, pp. 13–37.

[10]Fujita, T. T., "*DFW Microburst*, University of Chicago, IL, SMRP Research Paper 217, 1986 (NTIS PB 86-131638).

[11]Wingrove, R. C. and Bach, R. E. Jr., "Severe Winds in the DFW Microburst Measured from Two Aircraft," AIAA Paper 87-2340, Aug. 1987.

[12]Schultz, T. A., "A Multiple Vortex-Ring Model of the DFW Microburst," AIAA Paper 88-0685, Jan. 1988.

[13]Luers, J. K., "Wing Contamination: Threat To Safe Flight," *Journal of Astronautics and Aeronautics*, Nov. 1983, pp. 54–59.

[14]Dunham, R. E. Jr., Bezos, G. M., Gentry, G. L. Jr., and Melson, E. Jr., "Two-Dimensional Wind Tunnel Tests of a Transport-Type Airfoil in a Water Spray," AIAA Paper 85-0258, Jan. 1985.

[15]Dietenberger, M. A., Haines, P. A., and Luers, J. K., "Reconstruction of Pan Am New Orleans Accident," *Journal of Aircraft*, Vol. 22, Aug. 1985, pp. 719–728.

[16]Dunlap, E. W. and Porter, M. B., "Theory of the Measurement and Standardization of In-Flight Performance of Aircraft," Air Force Flight Test Center, Edwards, CA, Rept. FTC-TD-71-1, April 1971.

[17]Bach, R. E., Jr. and Parks, E. K., "Angle-of-Attack Estimation for Analysis of Windshear Encounters," *Journal of Aircraft*, Vol. 24, Nov. 1987, pp. 789–792.

[18]Bach, R. E., Jr., "A Variational Technique for Smoothing Flight-Test and Accident Data," *Journal of Aircraft*, Vol. 19, July 1982, pp. 546–552.